Natural ventilation by windcatchers: CFD simulations and experiments

Castillo, José Antonio*[1,2)], Huelsz, Guadalupe[1)], Cruz, Miriam Verónica[1)]

1) Instituto de Energías Renovables, Universidad Nacional Autónoma de México, Priv. Xochicalco s/n Col. Centro, Temixco Morelos, México.
2) Building Physics and Services, Eindhoven University of Technology, P.O. Box 513, 5600 MB Eindhoven, The Netherlands
**) presenting author, jacat@ier.unam.mx*

ABSTRACT

Natural ventilation can be improved by using a small structure on the roof, usually named windcatcher. This work presents the validation of computational fluid dynamics (CFD) simulations of the natural ventilation of a room with a windcatcher at the center of the roof; five different windcatcher configurations were analysed. Numerical simulations were performed using the software COMSOL and were validated using experimental results. Experiments were performed using a room scale model 1:25 in an open rectangular water channel. Stereoscopic Particle Image Velocimetry was used to measure the velocity vector field at the center plane of the room. A systematic procedure was employed to validate the numerical simulation with the experimental data. The average difference between experimental and numerical results of the wind speed a long the centreline of the room for all the windcatcher configurations is less than 10% and the difference between experimental and numerical results of the volumetric flow rate at the window is less to 7%.

1 INTRODUCTION

Natural ventilation on buildings by driven wind flow is an important passive strategy to promote indoor air quality, hygrothermal comfort and health; mainly in warm climates. If cross ventilation by windows is not viable or is insufficient, alternatives based on the modification of building roof can be used, given that the roof is often the most exposed part to the wind (Blocken et al., 2011; van Hooff et al., 2011). Hence, the research on natural ventilation in a room provided by a small structure raised on the roof, named windcatcher, is presented. The windcatcher experiments, usually, are performed under different settings and geometrical sections hindering comparison between them (Khan et al., 2008; Montazeri and Azizian, 2008; Hughes and Ghani, 2010; Montazeri et al., 2010; Montazeri et al., 2011; Saadatian et al., 2012). A set of windcatcher experiments, performed under same conditions (Cruz, 2013), were selected to validate the simulations of Computational Fluid Dynamics (CFD), by applying commercial software COMSOL 4.4. Although the experiments are the basis of CFD validation, CFD has advantages compared to most of the experimental techniques, including Stereoscopic Particle Image Velocimetry (SPIV). Because, CFD provides whole-flow field data, allows full control over the boundary conditions and enables easy parametric studies (Ramponi and Blocken, 2012; Blocken, 2014).

2 DESCRIPTION OF THE EXPERIMENTS

In the experiments, the room dimensions, the window geometry and location, the windcatcher position on the roof, the windcatcher height and cross section, and the wind speed were kept constant. The varied parameters were the windcatcher openings and the number of subducts. A typical room of a low-income-type house was considered, with interior dimensions 3.0m × 3.0m × 2.7m ($L_i \times W_i \times H_i$), with 0.15m of wall and roof thickness. The room had a window with

dimensions 1.30 m × 1.30 m (W_w × H_w). Figure 1 shows the five windcatcher configurations studied, all with square cross-section of 0.65m of length, with a parapet and an opening of 0.65 m height.

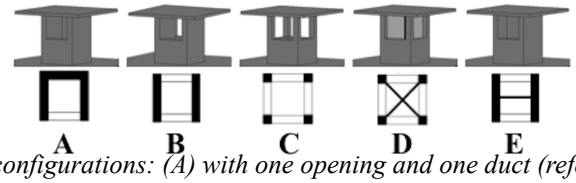

Figure 1*: Windcatcher configurations: (A) with one opening and one duct (reference case), (B) with two openings and one duct, (C) with four openings and one duct, (D) with four openings and four subducts, (E) with two openings and two subducts.*

The experiments were performed in an open rectangular water channel (ORWC) made with glass walls, of 6 m long, 0.315 m wide and 0.50 m height; the test section was 4.5 m from of the entrance. The room and the windcatchers were scaled to 1:25. The dynamic similarity was applied with Reynolds number $Re = U_{ref}H_r/\nu = 1.23 \times 10^4$ where $U_{ref} = 0.089$ m/s is the reference wind velocity at the scaled model height $H_r = 0.123$ m and $\nu = 8.94 \times 10^{-7}$m^2/s is the kinematic viscosity at the water temperature T_w = 25 ºC. Figure 2a illustrates the scaled model dimensions with windcatcher "A", which is taken as reference case. The scaled model was made of transparent acrylic of 6 mm for walls, of 9 mm for the floor, of 3 mm for the windcatcher roof and of 1mm for the windcatcher interior divisions. Velocity vector fields at central plane, measurement plane (Figure 2b), were taken with SPIV technique with resolution of 16 mm x 16 mm (64 x 64 pixels).

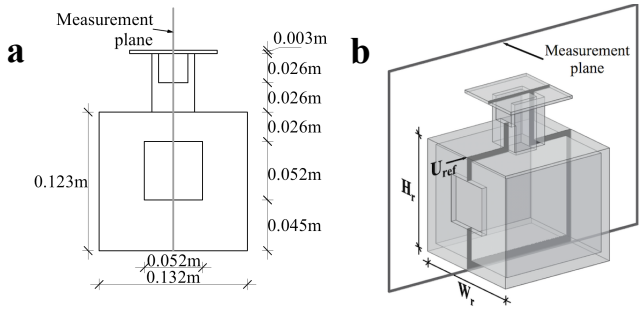

Figure 2*: Scaled model of a room with windcatcher "A" (Reference case): (a) Front view with dimensions; (b) Right isometric view with measurement plane.*

3 CFD SIMULATION: SETTINGS (REFERENCE CASE)

The simulations were performed with commercial CFD code COMSOL 4.4 (COMSOL, 2013). The 3D steady RANS equations were solved in combination with the shear-stress transport (SST) *k-ω* model. The GMRES solver with MULTIGRID-SOR preconditioner was employed for velocity-pressure coupling, and with MULTIGRID-SCGS preconditioner was used for viscous terms of the governing equations (COMSOL, 2013b). The convergence was assumed to be obtained when all the scaled residuals get a minimum of 10^{-6} (Ramponi and Blocken, 2012). A tetrahedral mesh was built with 1,176,225 nodes to simulate the empty ORWC. This empty ORWC domain was used to extract a tridimensional velocity profile, a turbulent kinetic energy (TKE) plane and a specific dissipation rate (SDR) plane; matching the velocity vertical profile computed with the experimental data measured at the test zone. The inlet boundary conditions were set according: the wind velocity profile defined by the logarithmic law, $U(z) = (u^*_{ABL}/\kappa)ln((z+z_0)/z_0)$, with the atmospheric boundary layer (ABL) friction velocity, u^*_{ABL} = 0.007m/s, the von Karman constant, $\kappa = 0.42$, the roughness length, $z_0 = 0.0005$ m, and the height coordinate, z. The TKE profile, $k(z) = (\sigma_u^2(z)+\sigma_v^2(z)+\sigma_w^2(z))/2$, was obtained from the standard deviation of velocity in the x-direction σ_u, the y-direction, σ_v, and the z-direction, σ_w. The turbulence dissipation rate (TDR) and SDR profiles were calculated, $\varepsilon(z)=u^{*3}_{ABL}/\kappa(z+z_0)$ and $\omega(z)$

$= \varepsilon(z)/C_\mu k(z)$, respectively, with the empirical constant $C_\mu = 0.09$ (Tominaga et al., 2008). The standard wall functions by COMSOL solver (COMSOL, 2013) were imposed on the ground surface and lateral walls. At the outlet plane, the zero static pressure was applied. The free slip condition at the top boundary, was applied, i.e. normal shear stress and pressure equals to zero.

3.1 Computational domain and grid

The short domain with reference case was built following guidelines by Tominaga et al. (2008) and Ramponi and Blocken (2012), which dimensions were $W_d \times L_d \times H_d = 0.315 \times 2.346 \times 0.41$ m^3 (Figure 3a). The computational grid A, formed by 853,224 tetrahedral cells (Figure 3b), was created.

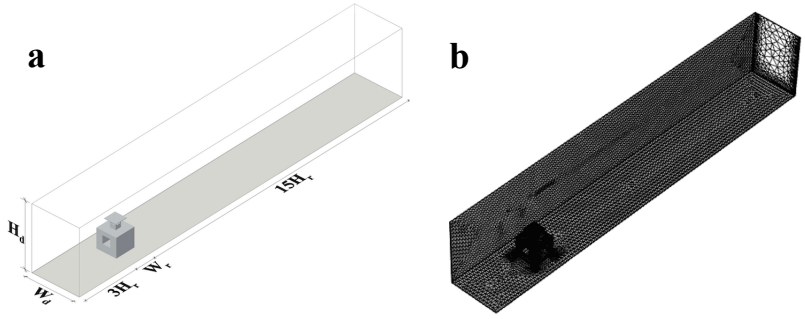

Figure 3*: Computational domain with the reference case: (a) Perspective view with dimensions of the domain; (b) Perspective view of grid at bottom, side and back face (Grid A with 853,224 cells).*

3.2 Boundary conditions

The tridimensional velocity profile, the TKE plane and the SDR plane, from the empty ORWC domain, were imposed as inlet conditions in the short domain. The standard wall functions (COMSOL, 2013) were imposed at ground surface and at lateral walls. The zero static pressure was applied on the rear face of the domain. The free slip condition at the top boundary was used. The streamwise gradients (Figure 4), which are an important quality criterion for the simulations (Blocken et al., 2007), were tested in the empty short domain. The test is to assess the extent of unintended streamwise gradients of the mean wind speed and the turbulence parameters, between the vertical profiles at inlet and at incident building position. In Figure 4, the inlet vertical profile (continuous line) and the incident vertical profile (dashed line) are presented. Minor streamwise gradients are observed.

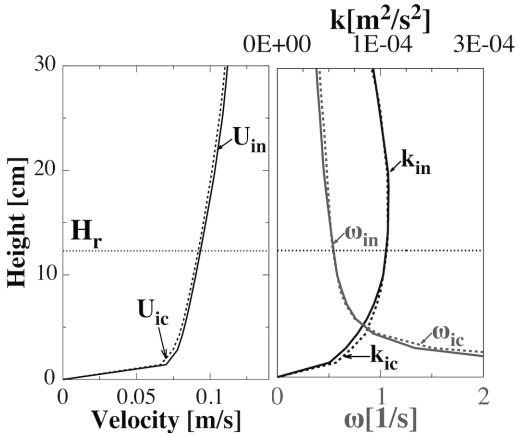

Figure 4*: Vertical profiles of (left) the mean wind speed, U; (right) the turbulent kinetic energy (dark line), k, and the specific dissipation rate (gray line), ω, at the inlet (continuous line) and at the incident building position (dashed line) in the empty domain. The subscripts "in" and "ic" refer to "inlet" and "incident", respectively. The height of the model (H_r) is 0.123 m (SST k-ω model, Grid A with 853,224 cells).*

3.3 Computational grid resolution

Three grids with 853,224 cells (grid A), 407,467 cells (grid B) and 287,655 cells (grid C) were constructed. The grids were obtained by coarsening the grid A twice by a factor of 2 (van Hooff and Blocken, 2010). The three grids of the reference case are illustrated in Figure 5.

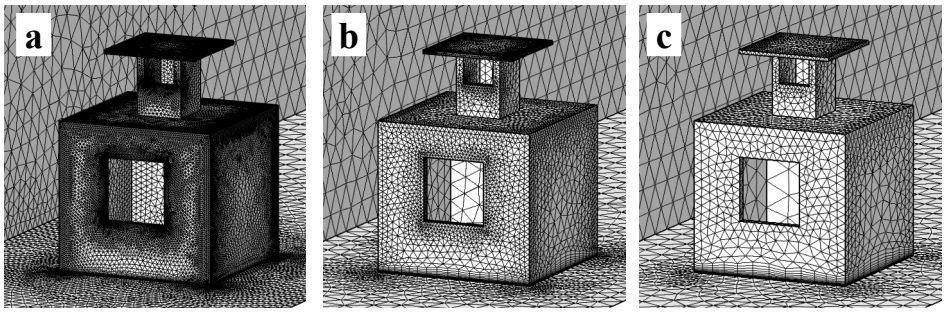

Figure 5: Isometric view of reference case: (a) Grid A with 853,224 cells; (b) Grid B with 407,467 cells; (c) Grid C with 287,655 cells.

In Figure 6, the grid sensitivity is small for the center line, L_r, before the inlet ($-0.25 \leq x/D_r < 0$) and from middle of the room to the rear wall ($0.5 \leq x/D_r < 1$). The difference of the wind speed ratio, u/U_{ref}, between the grid A and grid B at the room inlet is 0.80%, while between the grid B and grid C is 3.20%. The percentage average difference between the experimental, u_{SPIV} , and the numerical results, u_{CFD}, of the wind speed, $\Delta u = (|u_{SPIV}-u_{CFD}|/U_{ref})*100$, along L_r is for the Grid A 1.21% in the ranges $-0.25 < x/D_r \leq 0$ and $0.5 < x/D_r \leq 1$, and 4.39% for the range $0 < x/D_r \leq 0.5$. Therefore, the grid A (Fine) is a suitable grid to use. Even though, the numerical model tends to underestimate the mean velocity at the room inlet.

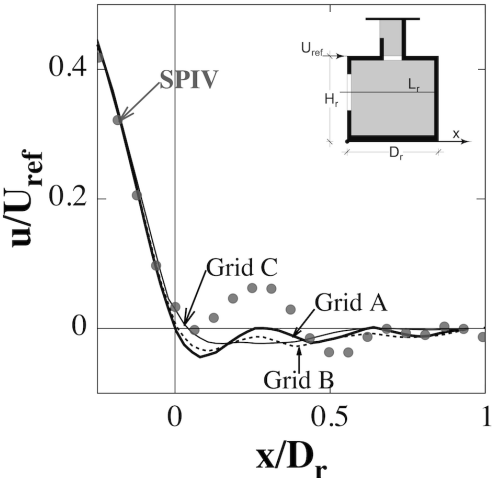

Figure 6: Grid sensitivity analysis of the reference case and comparison of the streamwise wind speed ratio u/U_{ref} along the centerline, L_r (reference case, SST k-ω model, 853,224 cells).

4 CFD SIMULATION: WINDCATCHERS

The simulations of the windcatcher configurations “B”, “C”, “D” and “E” were performed with the reference case settings (windcatcher A). In Figure 7, the centreplane velocity vector fields of all windcatcher configurations are shown, in left column from experimental data and in center column from numerical data. The streamwise wind speed ratio u/U_{ref} along L_r of all configurations are presented in right column of Figure 7. The letters of each row correspond to each windcatcher configuration (Figure 1).

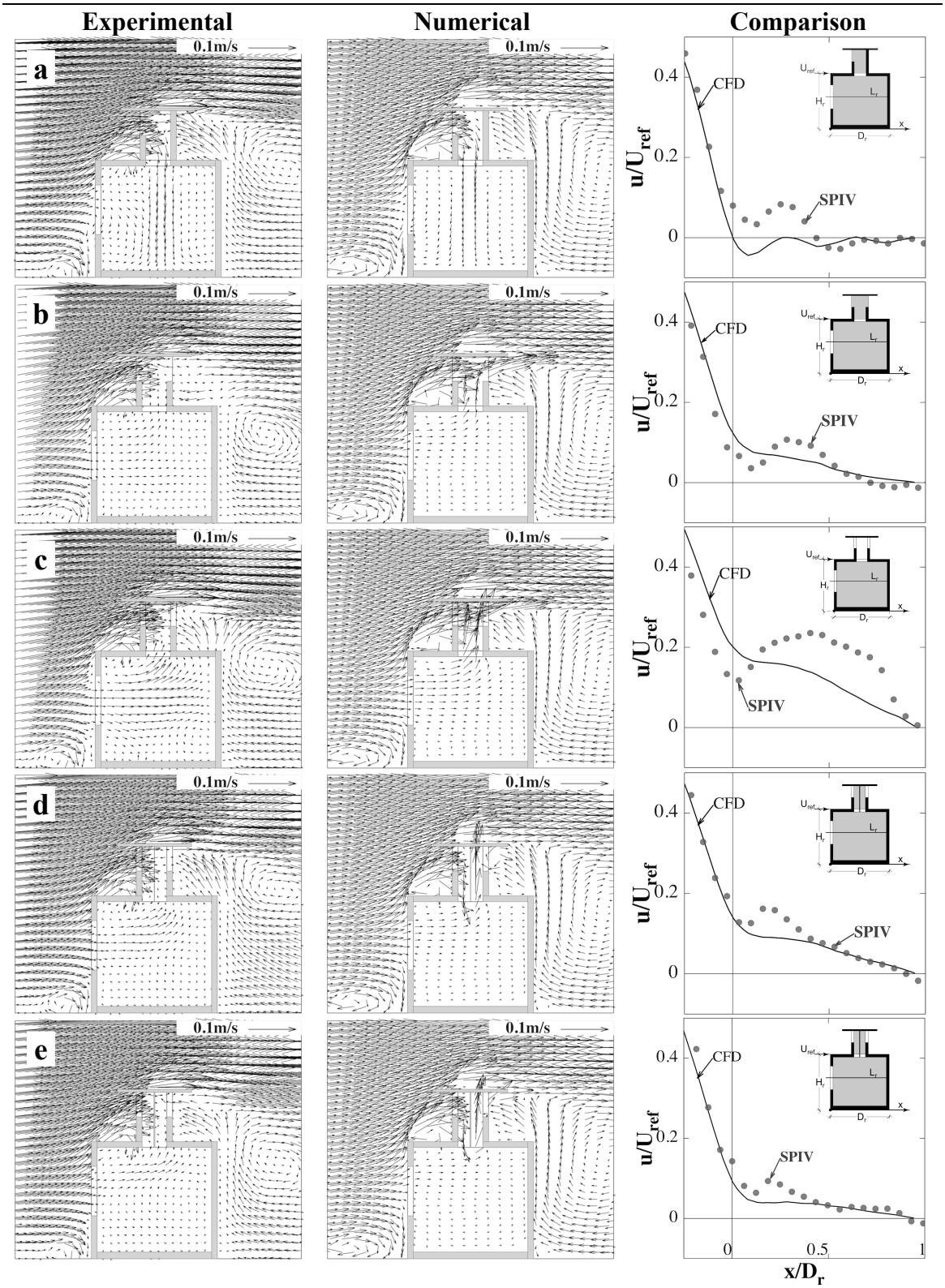

Figure 7: Velocity vector fields and streamwise wind speed ratio: (left column) The experimental field; (center column) The numerical; (right column) The comparison of streamwise wind speed ratio u/U_{ref} along the centerline between experimental and numerical results. The letter of each row defines the windcatcher configuration (Figure 1).

The central vector field show a close qualitative agreement between experimental and numerical results. The simulations reproduce the main vortexes of the flow, such as the one formed by the floor and the windward wall, the one formed by the roof and the windward wall, the one formed by the roof and the windcatcher base, and the biggest one in the rear of the room. The simulation tends to overestimate the structure size of the external vortexes round the scaled room. Besides, at interior of scaled room the simulation reduces the wind speed magnitude and the size of the structures. The percentage average difference between experimental and numerical results of the wind speed Δu of the windcatcher configurations are shown in Table 1. The windcatcher configuration "A" (reference case) presents the lower average value of 1.2% in the ranges $-0.25 < x/D_r \leq 0$ and $0.5 < x/D_r \leq 1$; while the other configurations have a value less to 4.3%, excepting the configuration "C" which exceeds the 7.0%. For the range $0 < x/D_r \leq 0.5$, the configuration "E" has the lower average value 2.4%, the configurations "A", "B" and "D" maintains a value over of 4.4% and the configuration "C" presents the highest value with 6.4%. In Table 1, the comparison of average difference of the wind speed Δu along the center line confirms the good match between the CFD results and SPIV measurements.

Table 1: Percentage average difference of the wind speed Δu between experimental data and numerical results along the center line.

Windcatcher configuration	Δu[%]	
	$-0.25 < x/D_r \leq 0$ $0.5 < x/D_r \leq 1$	$0 < x/D_r \leq 0.5$
(Ref. case) A	**1.2**	**4.4**
B	4.3	3.0
C	7.9	6.4
D	1.9	3.7
E	1.7	2.4

4.1 Volumetric flow rate

The volumetric flow rate entering to the window, $Q = UA$, is one of the most used parameters to evaluate the natural ventilation (ASHRAE, 2015), where U is the mean velocity normal to the window and $A = h \times w$ is the room window area with the height h and the width w. The experimental unitary flow rate, $Q_{SPIV}/w_u = h_i u_i$, was calculated assuming a unitary width w_u, with the normal velocity at the window of each vector u_i, and the discretized high h_i. A total of 9 vectors located at middle thickness of the window were considered. The numeric unitary flow rate, $Q_{CFD}/w_u = h_i u_i$, was calculated by discretizing the window height in 20 cells. The percentage unitary flow rate, $\Delta Q/w_u = |(Q_{SPIV}/w_u)-(Q_{CFD}/w_u)|/(Q_{ref}/w_u)*100$, was calculated with difference between experiment and simulation relative to the unitary reference flow rate, $Q_{ref}/w_u = hU_{ref}$. The Q_{SPIV}/w_u, Q_{CFD}/w_u and $\Delta Q/w_u$ were to evaluate the bidimensional ventilation phenomena. The experimental volumetric flow rate, $Q_{SPIV} = A_i u_i$, was calculated by summing the volumetric flow of each discretized area, $A_i = h_i \times w$, this implies the assumption that all the measured velocity at the central plane of the window does not change along to the window. The numerical volumetric flow rate, $Q_{CFD} = A_{ij} u_{ij}$, is the total sum of the volumetric flow rates evaluated in each one of the 400 cells at the middle thickness of the window; and the percentage difference between Q_{SPIV} and Q_{CFD} of the volumetric flow rate, $\Delta Q = |Q_{SPIV} - Q_{CFD}|/Q_{ref}*100$, was calculated with the reference volumetric flow rate, $Q_{ref} = AU_{ref}$. In Table 2, the unitary flow rates, the volumetric flow rates and the percentage differences at the window from experimental and numerical results are presented. The windcatcher configuration "A" (reference case) has a negative values for Q_{SPIV}/w_u, Q_{CFD}/w_u, Q_{SPIV} and Q_{CFD}, indicating a function as air inductor into the room; while the rest of configurations present a positive value, i.e. an extract function. The configurations "A" and "D" have the highest

values of Q_{SPIV}/w_u, -4.53 × $10^{-4} m^2/s$ and 4.72 × 10^{-4} m^2/s, respectively. Contrary, the configurations "C" and "D" have the highest values of Q_{CFD}/w_u, the highest values with 7.65 × $10^{-4} m^2/s$ and 4.87 × $10^{-4} m^2/s$, respectively. However, the configuration "A" and "C" present a value of $\Delta Q/w_u$ over 6%; while configuration "D" has the minimum values 0.3%, this configuration has the maximum promoter of flow rate into the room. The analysis for Q_{SPIV}, the configuration "A", "B" and "E" have a value lower than 1.85 × $10^{-5} m^3/s$, the configuration "D" presents the maximum value 2.45 × $10^{-5} m^3/s$. Moreover, the configuration "C" and "D" have for Q_{CFD} the highest values 3.66 × $10^{-5} m^3/s$ and 2.39 × $10^{-5} m^3/s$. However, the configuration "C" has for ΔQ the major value 6.6%. The flow rates comparison between bidimensional and tridimensional assumptions, gives the fundamentals to reject the volumetric flow rate calculation by a bidimensional approach.

Table 2: Unitary and volumetric flow rate at room window of the experimental and numerical results.

Windcatcher configuration	Unitary flow rate		$\Delta Q/w_u[\%]$	Volumetric flow rate		$\Delta Q[\%]$
	$Q_{SPIV}/w_u[m^2/s]$	$Q_{CFD}/w_u[m^2/s]$		$Q_{SPIV}[m^3/s]$	$Q_{CFD}[m^3/s]$	
(Ref. case) A	**-4.53 × 10^{-4}**	**-1.71 × 10^{-4}**	**6.1**	**-1.35 × 10^{-5}**	**-1.22 × 10^{-5}**	**0.5**
B	2.17 × 10^{-4}	3.75 × 10^{-4}	3.4	1.13 × 10^{-5}	1.70 × 10^{-5}	2.4
C	3.99 × 10^{-4}	7.65 × 10^{-4}	7.9	2.07 × 10^{-5}	3.66 × 10^{-5}	6.6
D	4.72 × 10^{-4}	4.87 × 10^{-4}	0.3	2.45 × 10^{-5}	2.39 × 10^{-5}	0.3
E	3.48 × 10^{-4}	2.63 × 10^{-4}	1.8	1.81 × 10^{-5}	1.15 × 10^{-5}	2.7

5 CONCLUSION

Numerical simulations, using the software COMSOL, of a room with different five windcatcher configurations were validated using experimental results from SPIV measurements. A systematic procedure was employed to validate the numerical simulation with the experimental data. The percentage average difference between experimental and numerical results of the wind speed a long the center line of the room for all the windcatcher configurations is less to 10% and the percentage difference between experimental and numerical results of the volumetric flow rate at the window is less to 7%. These numerical simulations can be used to verify the viability of the windcatcher in terms of air age, air changes and air mixing. Nevertheless, the implementation of other turbulence models is desirable to reduce the differences with the experimental data. Also, more accurate information from the experiments is recommended, i.e. velocity vector fields with more resolution and the velocity vector field at the window area.

Acknowledgements

The authors thank H. Cortés and M. Valdéz for computational technical support. Partial economic support from PAPIIT-UNAM IN113314 project is acknowledged. J.A. Castillo and M.V. Cruz acknowledge the scholarship given by CONACYT. The authors also wish to express their gratitude to prof. ir. Bert Blocken for the valuable comments on this work and to the Eindhoven University of Technology for providing the facilities.

References

ASHRAE, (2005). ASHRAE Handbook fundamentals. SI Edition, American Society of Heating, Refrigerating and Air Conditioning Engineers, Atlanta, EUA.

Blocken, B., Stathopoulos, T., Carmeliet, J. (2007). CFD simulation of the atmospheric boundary layer: wall function problems. Atmos Environ, Vol. 41, p238-252.

Blocken, B., van Hooff, T., Aanen, L., Bronsema, B. (2011). Computational analysis of the performance of a venturi-shaped roof for natural ventilation: Venturi-effect versus wind-blocking effect. Computers and Fluids, Vol. 48, p202–213.

Blocken, B. (2014). 50 years of Computational Wind Engineering: Past, present and future. Journal of Wind Engineering and Industrial Aerodynamics, accepted.

COMSOL (2013). CFD module user's guide, p654.

Cruz, M., V. (2013). Evaluation of ventilation passive systems. Unpublished master thesis (In Spanish), Institute of Renewable Energies UNAM, Mexico.

COMSOL (2013b). COMSOL Multiphysics Reference Manual, p1270.

Hughes, B., R., and Ghani, A. (2010). A numerical investigation into the effect of windvent louvre external angle on passive stack ventilation performance. Building and Environment , Vol. 45, p1025–1036.

Khan, N., Su, Y., and Riffat, S., B. (2008). A review on wind driven ventilation techniques. Energy and Buildings, Vol. 40, p1586–1604.

Montazeri, H., and Azizian, R. (2008). Experimental study on natural ventilation performance of one-sided wind catcher. Building and environment, Vol. 43, p2193–2202.

Montazeri, H., Montazeri, F., Azizian, R., Mostafavi, S. (2010). Two-sided wind catcher performance evaluation using experimental, numerical and analytical modeling. Renewable Energy, Vol. 35, p1424-1435.

Montazeri, H. (2011). Experimental and numerical study on natural ventilation performance of various multi-opening wind catchers. Building and Environment , Vol. 46, p370–378.

Ramponi, R., and Blocken, B. (2012). CFD simulation of cross-ventilation for a generic isolated building: Impact of computational parameters. Building and Environment , Vol. 53, p34–48.

Saadatian, O., Haw, L., C., Sopian, K. and Sulaiman, M., Y. (2012). Review of windcatcher technologies. Renewable and Sustainable Energy Reviews, Vol. 16, p1477–1495.

Tominaga, Y., Mochida, A., Yoshie, R., Kataoka, H., Nozu, T., Yoshikawa, M., et al. (2008). AIJ guidelines for practical applications of CFD to pedestrian wind environment around buildings. J Wind Eng Ind Aerodyn., Vol. 96, p1749–1761.

van Hooff, T., Blocken, B. (2010). Coupled urban wind flow and indoor natural ventilation modelling on a high-resolution grid: a case study for the Amsterdam Arena stadium. Environ Modell Softw, Vol. 25, p51-65.

van Hooff, T., Blocken, B., Aanen, A. and Bronsema, B. (2011). A venturi-shaped roof for wind induced natural ventilation of buildings: Wind tunnel and cfd evaluation of different design configurations. Building and Environment, Vol. 46, p1797–1807.